Backbone Dynamics of Inactive, Active, and Effector-Bound Cdc42Hs from Measurements of ^{15}N Relaxation Parameters at Multiple Field Strengths†

Adrienne P. Loh,‡ Wei Guo,§ Linda K. Nicholson,|| and Robert E. Oswald*,§

Department of Chemistry, University of Wisconsin−La Crosse, La Crosse, Wisconsin 54601, Department of Molecular Medicine, Cornell University, Ithaca, New York 14850, and Department of Molecular Biology and Genetics, Cornell University, Ithaca, New York 14850

Received June 15, 1999; Revised Manuscript Received July 29, 1999

ABSTRACT: Cdc42Hs, a member of the Ras superfamily of GTP-binding proteins, initiates a cascade that begins with the activation of several kinases, including p21-activated kinase (PAK). We have previously determined the structure of Cdc42Hs and found that the regions involved in effector (Switch I) and regulator (Switch II) actions are partially disordered [Feltham, J. L., et al. (1997) *Biochemistry 36*, 8755−8766]. Recently, we used a 46-amino acid fragment of PAK (PBD46) to define the binding surface on Cdc42Hs, which includes the β2 strand and a portion of Switch I [Guo, W., et al. (1998) *Biochemistry 37*, 14030−14037]. Here we describe the backbone dynamics of three constructs of [^{15}N]Cdc42Hs (GDP-, GMPPCP-, and GMPPCP- and PBD46-bound) using $^{15}N-^{1}H$ NMR measurements of T_1, $T_{1\rho}$, and the steady-state NOE at three magnetic field strengths. Residue-specific values of the generalized order parameters (S_s^2 and S_f^2), local correlation time (τ_e), and exchange rate (R_{ex}) were obtained using the Lipari−Szabo model-free formalism. Residues in Switch I were found to exhibit high-amplitude (low-order) motions on a nanosecond time scale, whereas those in Switch II experience low-amplitude motion on the nanosecond time scale and chemical (conformational) exchange on a millisecond time scale. The Insert region of Cdc42Hs-GDP exhibits high-order, nanosecond motions; the time scale of motion in the Insert is reduced in Cdc42Hs−GMPPCP and Cdc42Hs−PBD46. Overall, significant flexibility was observed mainly in the regions of Cdc42Hs that are involved in protein−protein interactions (Switch I, Switch II, and Insert), and flexibility was reduced upon interaction with a protein ligand. These results suggest that protein flexibility is important for high-affinity binding interactions.

The Ras superfamily of GTPases is a group of signal transduction proteins that are involved in a diverse variety of biological processes, including cell growth, differentiation, cytoskeletal organization, protein trafficking, and secretion (*1*). The exchange of GTP[1] for GDP places these proteins in an activated, signaling state, which is terminated by the hydrolysis of GTP to GDP by the intrinsic enzymatic activity of the protein. Ras proteins have become the subjects of intense investigation due in part to their connection with oncogenic processes (particularly members of the Ras subfamily such as H-Ras) (*2*, *3*). One such GTPase is Cdc42Hs, a member of the Rho subfamily. Cdc42Hs and H-Ras share a large degree of structural homology but are functionally distinct. For example, mutations that abolish the GTPase activity stimulate cell growth in H-Ras, but inhibit cell growth in Cdc42Hs (*4*). Rather, cell transformation by Cdc42Hs has been observed in mutants of Cdc42Hs that decreases its affinity for nucleotide and increases the GDP−GTP exchange rate (*5*). Furthermore, the regulators and effectors for H-Ras and Cdc42Hs are related but distinct proteins. To understand how these proteins can have such similar structures yet mediate different functional effects, it is necessary to characterize not only the structures but also the dynamic behaviors of these proteins on an atomic level as they interact with other molecules.

Cdc42Hs interacts with a variety of regulatory and effector proteins. Regulation is mediated by (a) Dbl and other guanine exchange factors (GEFs), which decrease the affinity for guanine nucleotides and promote the exchange of GDP for GTP (*4*, *6*, *7*), (b) GTPase activating proteins (GAPs), which stimulate the hydrolysis of GTP to GDP (*8*, *9*), and (c) a

† This work was supported by Grant R01 GM56233 from the National Institutes of Health.

* To whom correspondence should be addressed: Department of Molecular Medicine, College of Veterinary Medicine, Cornell University, Ithaca, NY 14853. Phone: (607) 253-3877. Fax: (607) 253-3659. E-mail: reo1@cornell.edu.

‡ University of Wisconsin−La Crosse.

§ Department of Molecular Medicine, Cornell University.

|| Department of Molecular Biology and Genetics, Cornell University.

[1] Abbreviations: Dbl, diffuse B-cell lymphoma; GDP, guanosine 5′-diphosphate; GTP, guanosine 5′-triphosphate; GMPPCP, β,γ-methylene derivative of GTP; GMPPNP, β,γ-imino derivative of GTP; aa, amino acid; PBD46, 46-amino acid portion of the Cdc42Hs binding domain of PAK; PAK, p21-activated kinase; GEF, guanine exchange factor; GDI, guanine nucleotide dissociation inhibitor; GAP, GTPase activating protein; Switch I, residues 31−40 of Cdc42Hs; Switch II, residues 57−74 of Cdc42Hs; Insert region, residues 118−134 of Cdc42Hs; HSQC, heteronuclear single-quantum correlation; NMR, nuclear magnetic resonance; NOE, nuclear Overhauser effect; T_1, longitudinal relaxation time; T_2, transverse relaxation time; $T_{1\rho}$, transverse relaxation time in the rotating frame; S^2, generalized order parameter; τ_e, local correlation time; τ_m, molecular or global correlation time; R_{ex}, chemical exchange rate.

10.1021/bi9913707 CCC: $18.00
Published on Web 09/08/1999

guanine nucleotide dissociation inhibitor (GDI), which detaches Cdc42Hs from the cellular membrane and inhibits GTP hydrolysis and GDP dissociation (*10*). Interactions between Cdc42Hs and regulator proteins involve three main sites on Cdc42Hs: Switch I, Switch II, and the Insert region. GAP binds to the two relatively disordered regions of Cdc42Hs termed Switch I and Switch II (*11*, *12*). GDI binds both to the prenylated C-terminus of Cdc42Hs (*13*) and to Switch II (G. R. Hoffman, N. Nassar, and R. A. Cerione, unpublished results; W. Guo, R. E. Oswald, and L. Y. Lian, unpublished results). However, GDI binds to but is ineffective in inhibiting GDP dissociation from mutants of Cdc42Hs that lack the Insert region, a region that is unique to the Rho subfamily of GTPases (*14*−*16*). In addition to its interaction with a variety of regulators, Cdc42Hs also interacts with a number of downstream effectors, one of which is p21-activated serine/threonine kinase (PAK). We have recently determined the solution structure of the GDP-bound form of Cdc42Hs (Cdc42Hs−GDP) using NMR spectroscopy (*17*). More recently, we have used a 46-residue peptide fragment of PAK (PBD46) to show that the Switch I and Switch II regions of Cdc42Hs−GMPPCP are involved in PAK binding (*18*) (W. Guo et al., unpublished results). These regions have also been shown to be involved in the binding of WASP (*19*) and ACK (*20*) effector proteins.

Previous studies suggest that Cdc42Hs possesses interesting dynamic characteristics. NMR studies of Cdc42Hs in the GDP-bound form (*17*) demonstrated that backbone resonances from three structural regions exhibited behaviors that were uncharacteristic of the remainder of the protein, suggesting increased flexibility. These same regions are those that are involved in protein−protein interactions: Switch I, Switch II, and the Insert region. In the case of Switch I and Switch II, the resonances of several amino acids broadened to the extent that they were not observable. In the case of the Insert region, few NOEs were observed relative to the remainder of the protein, and the backbone amide protons in the Insert helix were not protected from exchange to the same degree as helices in other regions of the protein. Similar results were obtained for the GMPPCP form (*17*). However, the Cdc42Hs construct that was bound to both GMPPCP and the effector fragment PBD46 appeared to be significantly more rigid, as evidenced by the observation of several previously unobserved residues in Switch I and Switch II (*18*).

In this paper, we characterize the backbone dynamics of Cdc42Hs in three different functional forms [inactive (GDP-bound), active (GMPPCP-bound), and effector-bound (GMPPCP- and PBD46-bound)] using $^{15}N-^{1}H$ NMR spectroscopy, with the ultimate goal of understanding the role of backbone flexibility in the function of Cdc42Hs. NMR spectroscopy is a particularly useful tool for investigating protein dynamics because it is sensitive to motion over a wide range of time scales (from picoseconds to milliseconds). Both global and local bond motions affect the relaxation rates of nuclear spins, and thus affect the line shapes of the NMR resonances. By measuring the longitudinal relaxation time (T_1), the transverse relaxation time (T_2 or $T_{1\rho}$), and the steady-state nuclear Overhauser effect (NOE) for each residue in the protein, information about the type and time scale of motion experienced by each residue can be obtained. This method has been used successfully for analyzing the dynamics of a number of proteins, including staphylococcal nuclease (*21*), HIV-1 protease (*22*), interleukin 1β (*23*), glucose permease (*24*), ubiquitin (*25*), and calmodulin (*26*).

Table 1: Measured Cdc42Hs ^{15}N Relaxation Parameters

	NOE	T_1			$T_{1\rho}$		
construct	600 MHz	600 MHz	500 MHz	400 MHz	600 MHz	500 MHz	400 MHz
Cdc42Hs−GDP	X	X	X		X	X	
Cdc42Hs−GMPPCP	X	X	X		X	X	X
Cdc42Hs−PBD46	X	X		X	X	X	X

EXPERIMENTAL PROCEDURES

Protein Preparation and Purification. The details of cell growth and protein purification procedures have been described previously (*18*). Briefly, uniformly ^{15}N-enriched Cdc42Hs was expressed as a hexahistidine-tagged protein in *Escherichia coli* strain BL21(DE3) from pET-15b-Cdc42Hs. This expression plasmid was subcloned to contain the 178 N-terminal amino acids (and a glycine, serine, and histidine which occur before the starting methionine) from the original pGEX-Cdc42Hs expression plasmid to improve the yield and to remove the unstructured C-terminal tail.

Three constructs of Cdc42Hs were examined: Cdc42Hs−GDP (one molecule of GDP bound to Cdc42Hs), Cdc42Hs−GMPPCP [one molecule of GMPPCP (a nonhydrolyzable analogue of GTP) bound to Cdc42Hs], and Cdc42Hs−PBD46 (one molecule of GMPPCP and one molecule of PBD46 bound to Cdc42Hs). The PBD46 peptide has been previously shown to be in slow exchange with Cdc42Hs−GMPPCP and to bind with an affinity of 20 nM (*18*).

NMR Spectroscopy. Protein samples were prepared in NMR buffer (25 mM NaCl, 5 mM NaH_2PO_4, 5 mM $MgCl_2$, and 1 mM NaN_3) with 10% D_2O at pH* 5.5 (no correction for isotope effects) at the following concentrations: 0.8 mM Cdc42Hs−GDP, 1.0 mM Cdc42Hs−GMPPCP, and 1.0 mM Cdc42Hs−PBD46 (*17*, *18*). Spectra were obtained on Varian Inova 600 MHz (Cornell Biomolecular NMR Center), Varian Unity 500 MHz (Cornell Chemistry NMR Facility), and Varian UnityPlus 400 MHz (Department of Biological Chemistry & Molecular Pharmacology, Harvard Medical School, Boston, MA) spectrometers (Table 1). All three spectrometers were equipped with triple-resonance pulsed-field gradient probes. Spectra were obtained at 25 °C in the States−TPPI mode (*27*, *28*) for quadrature detection. Chemical shifts were referenced as described previously (*17*).

Data were processed using NMRPipe version 1.6 (*29*) on a Sun Ultra 5 workstation, with preprocessing for sensitivity-enhanced experiments (*30*). Data were zero-filled to double the original number of data points, and apodized with a mixed exponential-Gauss window function. In all cases, numerical solvent suppression was applied prior to Fourier transformation, and a baseline correction was applied after Fourier transformation. Spectra were visualized and peak-picked using the PIPP suite of assignment programs (*31*).

^{15}N T_1 and $T_{1\rho}$ values were measured with sensitivity enhancement using 200 × 512 real data points at 16 scans

Table 2: Subsets of Dynamics Parameters ("Models") Used To Fit Experimental Relaxation Data to the Extended Lipari−Szabo Form of the Spectral Density Function

model	fit parameters	assumptions[a,b]	spectral density function	
1	S^2	$S_s^2 = 1$, $\tau_f \rightarrow 0$, $\tau_s \rightarrow 0$, $R_{ex} = 0$	$J(\omega) = {}^2/_5\{(S^2\tau_m)/[1 + (\omega\tau_m)^2]\}$	(2.1)
2	S^2 and τ_e	$S_s^2 = 1$, $\tau_e < \tau_m$, $R_{ex} = 0$	$J(\omega) = {}^2/_5\{(S^2\tau_m)/[1 + (\omega\tau_m)^2] + [(1 - S^2)\tau]/[1 + (\omega\tau)^2]\}$	(2.2)
3	S^2 and R_{ex}	$S_s^2 = 1$, $\tau_f \rightarrow 0$, $\tau_s \rightarrow 0$	$J(\omega) = {}^2/_5\{(S^2\tau_m)/[1 + (\omega\tau_m)^2]\}$	(2.3)
4	S^2, τ_e, and R_{ex}	$S_s^2 = 1$, $\tau_e < \tau_m$	$J(\omega) = {}^2/_5\{(S^2\tau_m)/[1 + (\omega\tau_m)^2] + [(1 - S^2)\tau]/[1 + (\omega\tau)^2]\}$	(2.4)
5	S_s^2, S_f^2, and τ_e	$\tau_f \rightarrow 0$, $\tau_e < \tau_m$, $R_{ex} = 0$	$J(\omega) = (2S_f^2/5)\{(S_s^2\tau_m)/[1 + (\omega\tau_m)^2] + [(1 - S_s^2)\tau]/[1 + (\omega\tau)^2]\}$	(2.5)

[a] In models 1, 3, and 5, τ_f is assumed to be small enough (<10 ps) that it makes a negligible contribution to the relaxation parameters. In models 2 and 4, $\tau_e = \tau_f$ (there is no slow component). [b] In models 1−4, $S^2 = S_f^2$. The value of the order parameter (S^2) ranges from 0, which represents completely isotropic local motion, to 1, which represents completely restricted local motion. A τ_e value of 0 implies that local motions are very fast (<10 ps). A τ_e value equal to τ_m implies that local motions are too slow to be distinguished from molecular motion.

per point, using pulse sequences described elsewhere (*32*, *33*). $T_{1\rho}$ data were obtained using continuous ^{15}N spin locking (*34*). Eight to nine relaxation delay points were used to define each decay curve; delay times were in the range of ∼12−1000 ms for T_1, and ∼8−100 ms for $T_{1\rho}$. Peak volumes were determined by fitting a Gaussian line shape to the experimental peak using the program nlinLS (*29*). Relaxation times (T_1 or $T_{1\rho}$) were then obtained using conjugate gradient minimization and Monte Carlo simulation to fit the relaxation delay points to an exponential decay function with a time constant T_i and zero intercept (*22*). Errors in relaxation times (expressed as standard deviations) were chosen as the larger of those either from the exponential fit or from a duplicate pair of relaxation delay points. ^{15}N−^{1}H NOE values were measured with 200 × 512 real data points at 32 scans per point, using inverse detection and a water flip back pulse scheme (*35*). Each NOE value was determined from the ratio of peak volumes in the presence and absence of proton saturation. Standard deviations in the NOE values were determined from the rms baseline noise as described by Nicholson et al. (*36*).

$T_{1\rho}$ values were corrected for off-resonance effects using the relation (*37*, *38*)

$$\frac{1}{T_{1\rho}} = \frac{1}{T_1}\cos^2\theta + \frac{1}{T_2}\sin^2\theta \quad (1)$$

where $1/T_{1\rho}$ and $1/T_2$ are the uncorrected and corrected transverse relaxation rates (including chemical exchange effects), respectively. The tip angle, θ, is given by

$$\theta = \arctan\left(\frac{B_0\Delta\delta}{B_1}\right) \quad (2)$$

in which B_1 is the spin lock field strength (2.5 kHz), B_0 is the ^{15}N static field strength in megahertz, and $\Delta\delta$ is the chemical shift offset from the carrier frequency, in parts per million. Values of T_2 calculated from eq 1 were used in all data analyses. Since the corrections were small (<5% in most cases), errors in T_2 were taken to be the same as those in $T_{1\rho}$.

Theory and Data Analysis. The ^{15}N relaxation parameters T_1, T_2, and NOE can be expressed in terms of the spectral density function $J(\omega)$, using the fact that relaxation of an ^{15}N nucleus attached to an ^{1}H nucleus is dominated by chemical shift anisotropy and ^{1}H−^{15}N dipolar interaction mechanisms (*39*, *40*):

$$\frac{1}{T_1} = \frac{d^2}{4}[J(\omega_H - \omega_N) + 3J(\omega_N) + 6J(\omega_H + \omega_N)] + c^2J(\omega_N) \quad (3)$$

$$\frac{1}{T_2} = \frac{d^2}{8}[4J(0) + J(\omega_H - \omega_N) + 3J(\omega_N) + 6J(\omega_H) + 6J(\omega_H + \omega_N)] + \frac{c^2}{6}[4J(0) + J(\omega_N)] + R_{ex} \quad (4)$$

$$\mathrm{NOE} = 1 + \frac{d^2T_1\gamma_H}{4\gamma_N}[6J(\omega_H + \omega_N) - J(\omega_H - \omega_N)] \quad (5)$$

where γ_i is the gyromagnetic ratio of nucleus i, $d = (\mu_o h\gamma_N\gamma_H/8\pi^2 r_{NH}^3)$, $c = \omega_N\Delta\sigma/\sqrt{3}$, μ_o is the permeability of free space, h is Planck's constant, r_{NH} is the ^{15}N−^{1}H bond length [assumed to be 1.02 Å (*41*)], and $\Delta\sigma$ is the chemical shift anisotropy [assumed to be −160 ppm (*42*)]. The R_{ex} term in eq 4 accounts for any additional relaxation that may occur through chemical exchange. The rate of chemical exchange is proportional to $(\Delta\omega)^2$, where $\Delta\omega$ is the chemical shift difference between the two exchange states, and thus depends on the square of the external field strength (*43*, *44*). Therefore, particular care was taken to measure $T_{1\rho}$ values at more than one field (Table 1).

If the molecular motion is assumed to be isotropic, the spectral density function for each ^{15}N nucleus can be approximated using the "model-free" formalism developed by Lipari and Szabo (*40*, *45*) and extended by Clore et al. (*46*). In the most general form, the spectral density function is given by

$$J(\omega) = {}^2/_5\left[\frac{S^2\tau_m}{1 + (\omega\tau_m)^2} + \frac{(S_f^2 - S^2)\tau_s'}{1 + (\omega\tau_s')^2} + \frac{(1 - S_f^2)\tau_f'}{1 + (\omega\tau_f')^2}\right] \quad (6)$$

where

$$\tau_i' = \frac{\tau_i\tau_m}{\tau_i + \tau_m} \quad (7)$$

where ω is the Larmor frequency of the ^{15}N nucleus, τ_m is the global correlation time, which characterizes the time scale of molecular tumbling, τ_i is the local correlation time

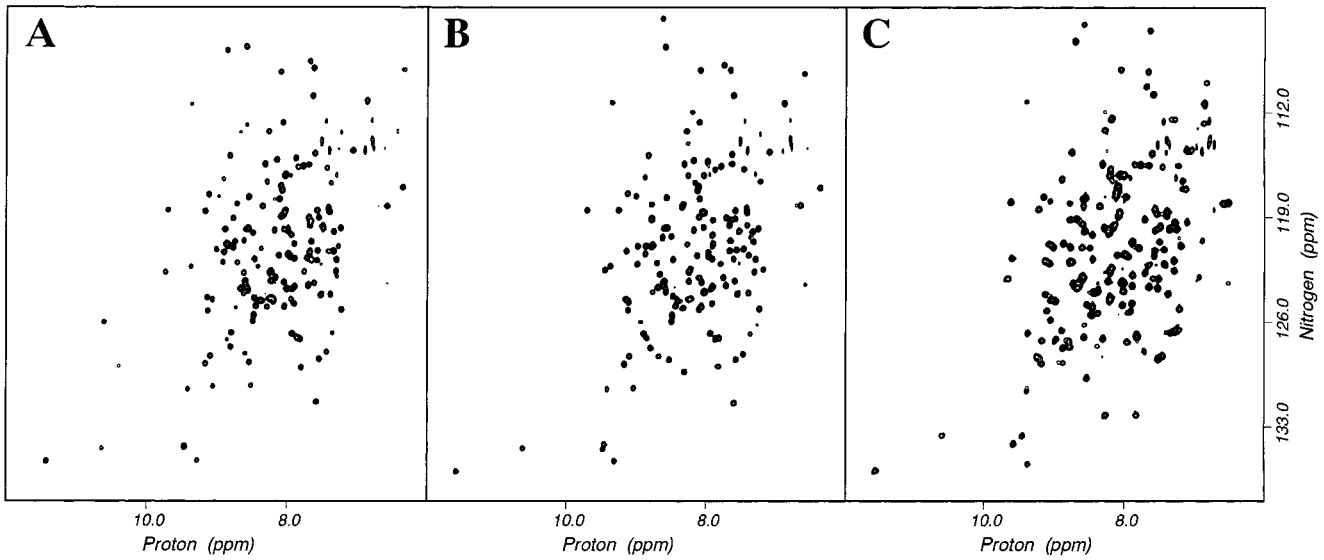

FIGURE 1: Sample $^{15}N-^{1}H$ HSQC (*67*) spectra of (A) Cdc42Hs−GDP, (B) Cdc42Hs−GMPPCP, and (C) Cdc42Hs−PBD46, obtained at 600 MHz using the $T_{1\rho}$ pulse sequence with a relaxation delay of 8.0 ms. Only Cdc42Hs is uniformly ^{15}N-labeled; therefore, PBD46 resonances do not appear in spectrum C. There are only 19 unassigned non-proline residues in Cdc42Hs−GDP; the majority of the unassigned residues occur in the Switch regions, loops, or termini of the protein: M1, several residues in Switch I (V36−A41), several residues in Switch II (D57−R68), and V14, T75, E91, and T108. In Cdc42Hs−GMPPCP, there are 16 unassigned non-proline residues: the same residues in Switch I (V36−A41), fewer residues in Switch II (D57−Q61 and R68), and V14, G15, K107, and T108. In Cdc42Hs−PBD46, there are only 10 unassigned non-proline residues: D11, A13−K16, only one residue in Switch I (T35), and only a few residues in Switch II (G60, Q61, R66, and L67). The 12 proline residues cannot be observed using proton-detected $^{15}N-^{1}H$ HSQC spectroscopy.

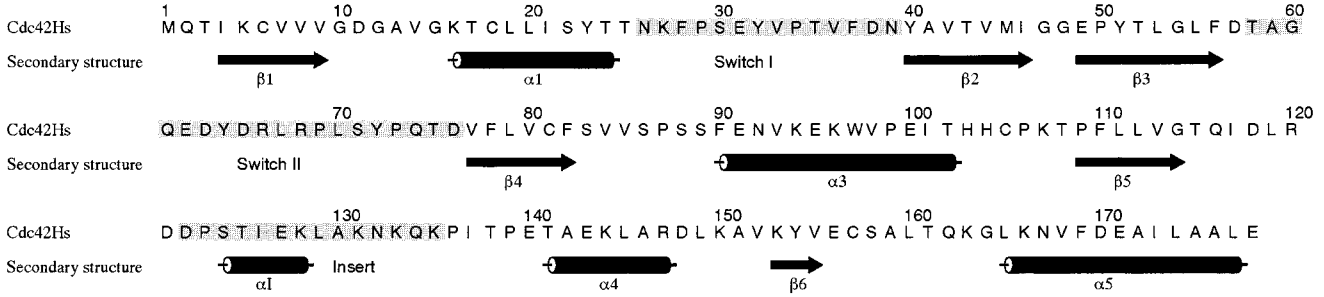

FIGURE 2: Amino acid sequence of Cdc42Hs. The secondary structure components determined from the NMR structure of Cdc42Hs−GDP are also indicated (*17*). [This figure was produced using the program ALSCRIPT (*68*).]

describing motion on a slow (s) or fast (f) time scale relative to τ_m ($\tau_f < \tau_s < \tau_m$), and S^2 ($=S_s^2S_f^2$) is the generalized order parameter, which describes the degree of restriction (or amplitude) of the local $^{15}N-^{1}H$ bond motions. Three simpler forms of the spectral density function were considered for data analysis (Table 2) as described by Mandel et al. (*47*). For each residue, the simplest model that fit the data was used (see below).

Values for the dynamics parameters S_f^2, S_s^2, τ_e, and R_{ex} for all residues were obtained by fitting the experimental relaxation data at all fields to the appropriate form of the spectral density function using the software package Modelfree, version 4.0 (*48*). All five models were considered for each residue. For each model, 300 randomly distributed synthetic data sets were generated from the experimental relaxation parameters assuming a Gaussian distribution of experimental errors. These simulations were used to determine the errors (expressed as standard deviations) in the dynamics parameters. The quality of the fit was evaluated using a χ^2 comparison of the calculated and experimental relaxation parameters (eq 8, where the sum extends over the M measurements of the relaxation parameters at different field strengths).

$$\chi^2 = \sum_M \left[\frac{(R_1^{\exp} - R_1^{\text{calc}})^2}{\sigma_1^2} + \frac{(R_2^{\exp} - R_2^{\text{calc}})^2}{\sigma_2^2} + \frac{(\text{NOE}^{\exp} - \text{NOE}^{\text{calc}})^2}{\sigma_{\text{NOE}}^2} \right] \quad (8)$$

Values of R_1^{calc}, R_2^{calc}, and NOE^{calc} were back-calculated from the fit values of the dynamics parameters. The most appropriate model for each residue was chosen on the basis of an F-test criterion, in which values of F_{obs} [$=(\chi_i^2/\nu_i)/(\chi_j^2/\nu_j)$] were compared to the limiting values of $F(\nu_i,\nu_j)$ at 90% confidence, where ν_i ($=m - n$) is the number of degrees of freedom in that particular model, m is the number of experimental relaxation parameters, n is the number of fit parameters, and χ^2 is calculated from eq 8. A more complicated model (more fit parameters) was chosen only if the reduction in the value of the reduced χ^2 (χ^2/ν) was significant at the 90% confidence level (*49*).

Values for τ_m for each construct were obtained from a grid search using a filtered average of T_1/T_2 values measured at 600 MHz. Briefly, a value of T_1/T_2 was calculated for each residue. Residues with T_1/T_2 values outside of the 67%

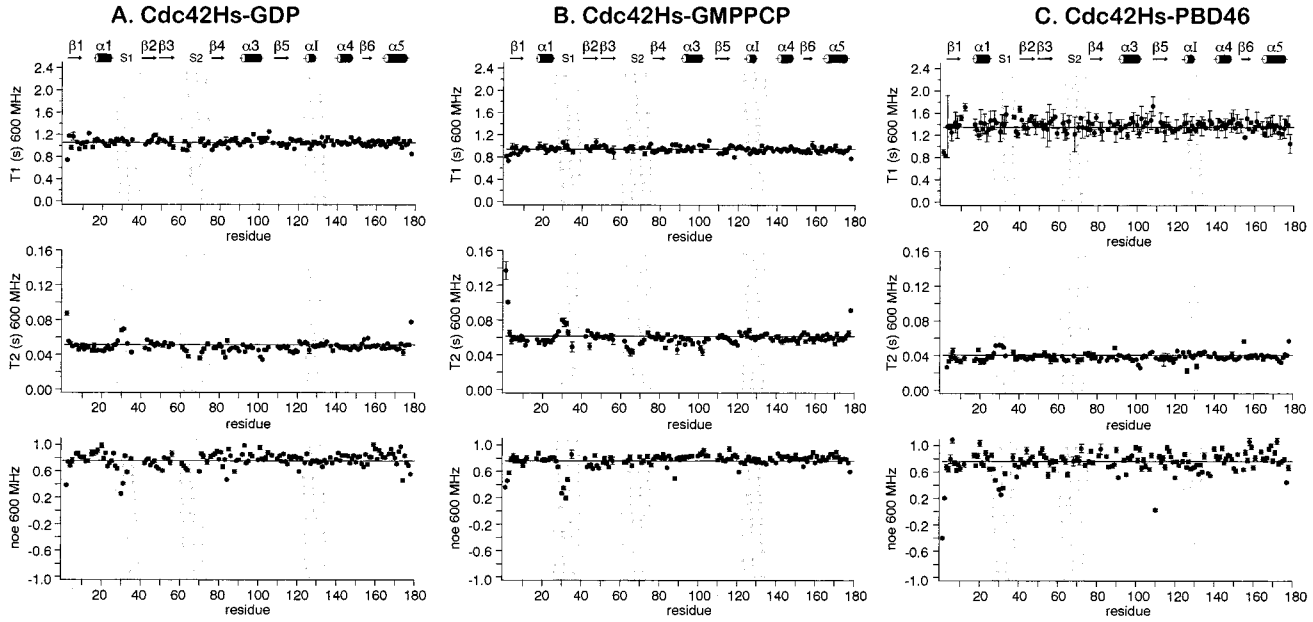

FIGURE 3: Relaxation data for the three constructs of Cdc42Hs, measured at 600 MHz. For the GDP construct, relaxation parameters for four residues (C6, L19, L53, and V98) could not be obtained due to spectral overlap. Relaxation parameters were also obtained for all but four residues in the GMPPCP construct (K16 was too weak to observe in the latter time slices, A13 and L19 were weak and overlapped with other spectral peaks, and L67 was fit only with large error). For the PBD46 construct, relaxation parameters could be obtained for all but eight residues (V36 and S83 were too weak to observe in the latter time slices, and V80, V84, V93, L111, Y154, and K163 were obstructed by severe spectral overlap). The increased level of congestion in the Cdc42Hs−PBD46 spectra is not surprising as the PBD46 ligand adds 46 residues to the total mass of the construct, changing the global tumbling time τ_m (see Table 4).

confidence interval (one standard deviation) were excluded, as were residues with NOE values below 0.65. The excluded residues represent those which strongly contribute to the relaxation rates and/or have significant chemical exchange or other (nonmodeled) relaxation components (*21*, *22*). The experimental relaxation values (at all measured fields) for the *N* residues that survived the filter were fit to the simple Lipari−Szabo version of eq 6 (model 2 in Table 2), assuming a fixed value of τ_m at each step, until the value of the total χ^2 was minimized. The 90% confidence interval for τ_m was taken as the range of τ_m encompassed by the 90% confidence interval for χ^2 ($\Delta\chi^2 \leq 2.71N$) (*22*).

To determine if asymmetry in the protein structure contributes significantly to the values of the calculated parameters and the choice of model, relaxation data (at both fields) for the GDP construct were also fit to models 1−5 using the axially symmetric anisotropic version of Modelfree, version 4.0 (*48*). The anisotropic diffusion tensor was determined using the program R2R1_diffusion (*48*) with atomic coordinates from the NMR solution structure (*17*) and a filter constructed from the T_1/T_2 ratio at 600 MHz as described above [residues that were found to experience chemical exchange using the isotropic model and residues that produced extremely high χ^2 values in the first iteration (C18, L20, K96, S124, and K166) were also excluded]. On the basis of the 91 residues that survived this filter, the anisotropic ratio ($D_{||}/D_{\perp}$) was found to be 1.137. Data analysis was the same as for the isotropic model fits, as described above.

RESULTS

NMR Data

Sample $^{15}N-^{1}H$ HSQC spectra and the Cdc42Hs sequence are shown in Figures 1 and 2, respectively. The three functional regions of the protein have been identified as residues 31−40 (Switch I), residues 57−74 (Switch II), and residues 118−134 (Insert). Sequence assignments of the backbone N−H resonances have been previously published for all three constructs of Cdc42Hs (*17*, *18*). Of the 178 residues in the truncated protein, only 19 non-proline residues remained unassigned in Cdc42Hs−GDP, 16 residues remain unassigned in Cdc42Hs−GMPPCP, and 10 residues remain unassigned in Cdc42Hs−PBD46. The increased number of assignments for Cdc42Hs−PBD46 in the Switch regions is an initial indication of decreased motional line broadening versus the GDP and GMPPCP forms.

Values for the relaxation parameters T_1, T_2, and NOE were obtained from a combination of Gaussian line shape fits and exponential decay fits. In some cases, reliable values for the relaxation parameters could not be obtained either because the signals were too weak to be observed in latter time slices or because there was severe spectral overlap. In total, relaxation parameters were obtained for 143, 146, and 148 of the 166 non-proline residues in Cdc42Hs−GDP, −GMPPCP, and −PBD46, respectively.

Values for T_1, T_2, and NOE obtained at 600 MHz for the three constructs of Cdc42Hs are shown in Figure 3. While there is very little variation in the value of T_1 across the sequence of Cdc42Hs (see below), the T_2 values suggest clear differences between the bulk of the protein and several regions of Cdc42Hs. In particular, T_2 rises significantly above the mean (Table 3) at Switch I in the GDP and GMPPCP constructs, but rises very little in the same region in the PBD46 construct. A rise in T_2 is also observed at the N- and C-termini of all constructs. In contrast, T_2 drops below the mean at Switch II for the GDP and GMPPCP forms, while there is no noticeable deviation from the mean at Switch II for the PBD46 form. A drop in T_2 for all three forms is also observed for residues 97−102, which comprise

Table 3: Average Values of Relaxation Parameters for the Three Constructs of Cdc42Hs

	NOE	T_1 (ms)			T_2 (ms)		
construct	600 MHz	600 MHz	500 MHz	400 MHz	600 MHz	500 MHz	400 MHz
Cdc42Hs−GDP	0.761 ± 0.022	1055 ± 21	723 ± 67		49.2 ± 1.4	52.6 ± 2.1	
Cdc42Hs−GMPPCP	0.755 ± 0.188	944 ± 66	705 ± 55		60.3 ± 1.5	62.6 ± 2.2	68.3 ± 3.8
Cdc42Hs−PBD46	0.761 ± 0.034	1347 ± 32		611 ± 34	39.5 ± 1.6	44.0 ± 2.6	48.4 ± 3.0

Table 4: Molecular (Global) Correlation Times and Average Values of the Fast and Slow Time Scale Order Parameters for Cdc42Hs

construct	S_f^2	S_s^2	τ_m (ns)
Cdc42Hs−GDP	0.952 ± 0.010 (143 aa)	0.912 ± 0.009 (20 aa)	14.8 ± 0.4
Cdc42Hs−GMPPCP	0.941 ± 0.010 (145 aa)	0.892 ± 0.010 (15 aa)	12.6 ± 0.2
Cdc42Hs−PBD46	0.946 ± 0.015 (148 aa)	0.841 ± 0.018 (1 aa)	18.6 ± 0.5

one face of the α3 helix (Figures 3 and 5). Deviations in T_2 are reflected in part in the NOE values. Residues with high T_2 values have low NOE values. However, residues that have low T_2 values have average (GMPPCP) or slightly below average (GDP) NOE values. Overall, there appear to be two groups of residues that have relaxation parameter characteristics different from those of the bulk of the protein: (1) residues with higher-than-average T_2 values and lower-than-average NOE values in all three constructs (i.e., Switch I and the ends of the protein) and (2) residues with lower-than-average T_2 values and average or below-average NOE values (i.e., Switch II and some of helix α3 in the GDP and GMPPCP forms).

Backbone Dynamics

Values of the parameters that characterize the global (τ_m) and residue-specific (S_f^2, S_s^2, τ_e, and R_{ex}) dynamics of Cdc42Hs were obtained by fitting the relaxation data to five different dynamics models (Table 2). Each model comprises a subset of the dynamics parameters included in the extended Lipari−Szabo model-free formalism. For each residue, the best model was identified as the one that produced the best fit between the experimental and calculated values for the relaxation parameters, as judged by a combination of the reduced χ^2 values and an F test (see Experimental Procedures). In a few cases, the best fit model produced τ_e values that reached the upper bound (τ_m), or had very high error (>100%). These fits indicate that local motion at these residues is difficult to model accurately.

Molecular correlation times (τ_m) for the three constructs are listed in Table 4. The large τ_m for Cdc42Hs−PBD46 can be attributed to an increase in the mass of the construct due to the addition of the 46-amino acid peptide. Residue-specific values of the dynamics parameters and best-fit models are shown in Figures 4 and 5, respectively.

Switch I. In all three forms, the order parameter ($S^2 = S_f^2 S_s^2$) drops below the mean (Table 4) at Switch I and at the ends of the protein, indicating reduced order (increased amplitude of motion). This is consistent with the observation that these same residues exhibited higher-than-average T_2 values, and lower-than-average NOE values. Residues in Switch I were generally best fit by models that included motion on either one (model 2, green in Figure 5) or two

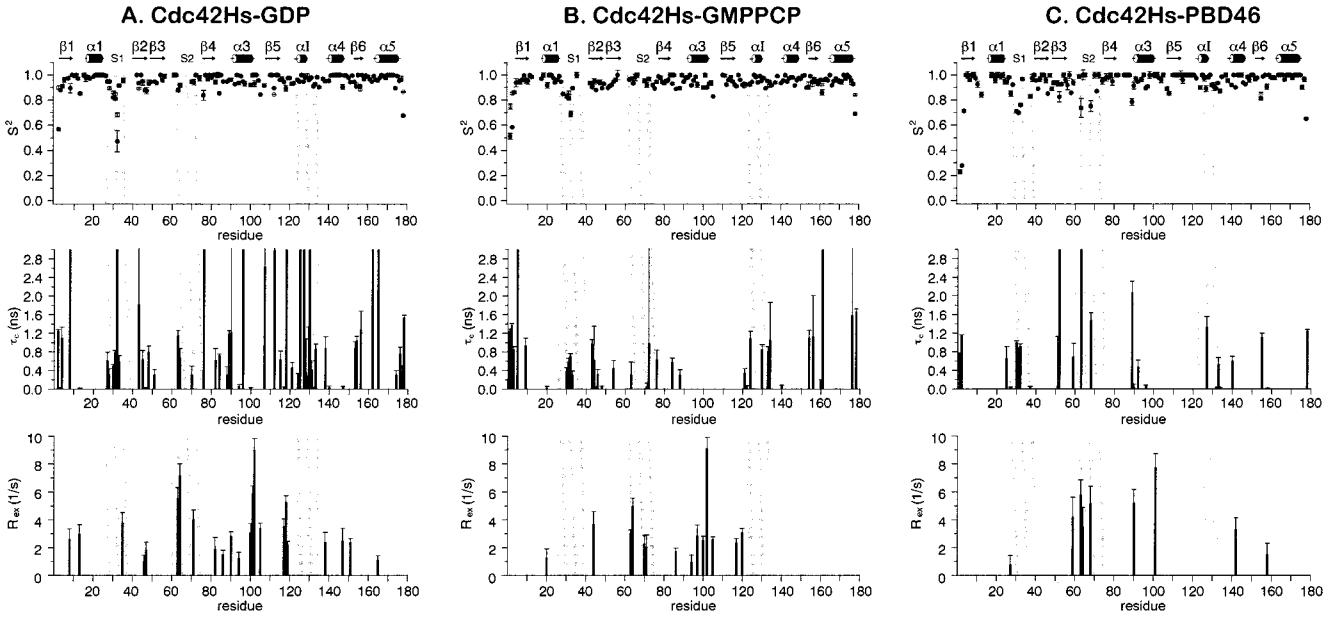

FIGURE 4: Dynamics parameters extracted using the extended Lipari−Szabo model-free formalism for the three constructs of Cdc42Hs. (Top panels) S_f^2 (●) and S_s^2 (○). Values for R_{ex} are reported at 600 MHz. In a few cases, the best fit model produced τ_e values that reached the upper bound of τ_m (for GDP: Y32, D76, and Q162; for GMPPCP: K5 and T161; and for PBD46: T52 and D63) or had very high error (>100%) (for GDP: F90, K107, K128, L129, and L165; for GMPPCP: T44, S71, Y72, and A176; and for PBD46: F90 and Y51). These fits indicate that local motion at these residues is difficult to model accurately. Some values of τ_e are off-scale in the above plots: (A) residue 8, $\tau_e = 9.85 \pm 3.58$ ns; residue 76, $\tau_e = 13.7 \pm 4.0$ ns; residue 96, $\tau_e = 8.96 \pm 0.66$ ns; residue 112, $\tau_e = 2.99 \pm 0.04$ ns; residue 118, $\tau_e = 10.2 \pm 3.2$ ns; residue 125, $\tau_e = 11.1 \pm 2.4$ ns; residue 130, $\tau_e = 7.97 \pm 0.67$ ns; and residue 165, $\tau_e = 3.60 \pm 3.59$ ns; and (C) residue 52, $\tau_e = 14.6 \pm 5.9$ ns; and residue 63, $\tau_e = 17.6 \pm 5.8$ ns.

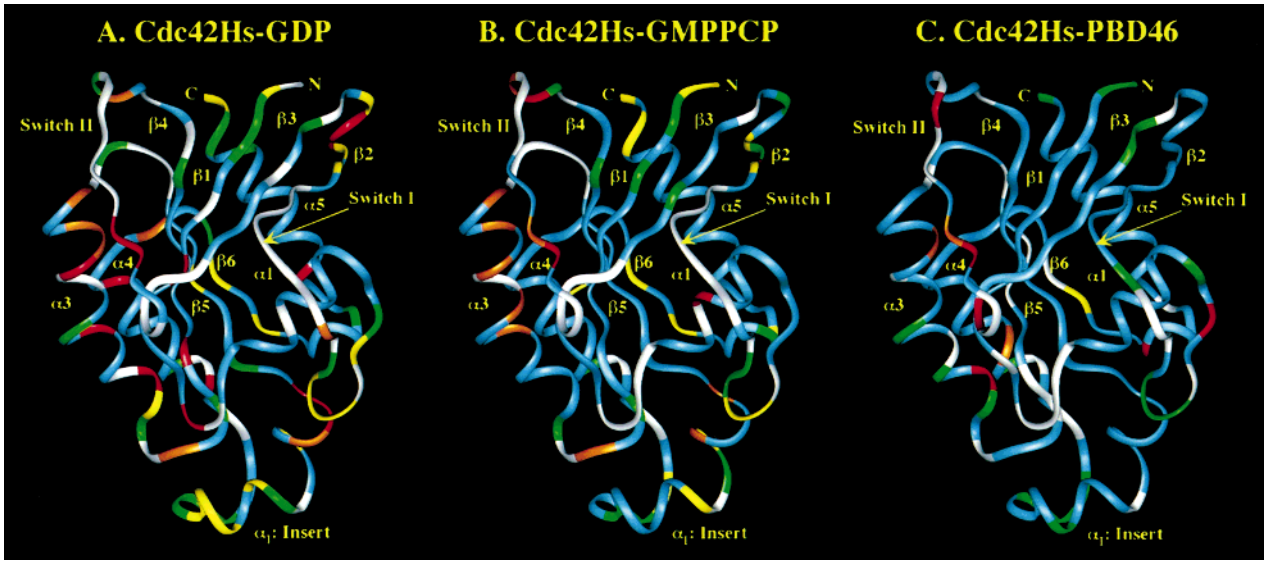

FIGURE 5: Best fit models for the three constructs of Cdc42Hs: white, unassigned; blue, model 1; green, model 2; yellow, model 5; orange, model 3; and red, model 4.

(model 5, yellow in Figure 5) time scales, with observed correlation times on the order of 1 ns (Figure 4). The low order parameters associated with the observable residues at either end of Switch I suggest that the residues in the middle of Switch I that were not observable (white, Figure 5) are also likely to be flexible and experience high-amplitude motions on the nanosecond to picosecond time scale. The absence of these peaks in the NMR spectrum is most probably due to additional motion on the millisecond time scale, producing severe line broadening (*17*).

Binding of PBD46 affects the dynamics of Switch I considerably, as evidenced by the increased number of residues that were observable in the NMR spectrum (less white, Figure 5) and the reduction in the complexity of the models required to fit the data (primarily models 1 and 2 rather than model 5). This is not surprising given that PBD46 binds to Cdc42Hs near Switch I and is likely to impose steric constraints on local motion. Nevertheless, it is interesting to note that the drop in S^2 relative to that of the remainder of the protein persists in the PBD46 form, and that the time scale of motion does not change. Evidently, Switch I remains partially disordered even upon binding of PBD46.

One might expect that the decrease in the order parameter at Switch I would be reflected in the values of T_1 for these residues. However, Figure 3 shows that the values of T_1 do not deviate from the protein average in this region. This may be explained by examining the dependence of T_1 on the order parameter and local correlation time. T_1 is insensitive to dynamics when S^2 is large (greater than ~0.85 in this case) and when motions occur on a time scale near the intersection point of the T_1 versus τ_e plot ($\tau_{critical}$) (*50*). The value of $\tau_{critical}$ depends on the molecular correlation time, and is equal to ~200, 275, and 150 ps for the GDP, GMPPCP, and PBD46 constructs, respectively. Accurate determination of τ_e for proteins with large τ_m values is very difficult and is influenced significantly by even small experimental errors in T_1 (*50*, *51*). Therefore, it is likely that the errors in the fit values of τ_e are in actuality larger than those reported and encompass $\tau_{critical}$. (The invariance of T_1 across the remainder of the protein can be explained by high order parameters.)

Switch II. In contrast to what is observed for Switch I, no noticeable deviation from the mean values of S^2 is observed at Switch II for the GDP or GMPPCP constructs. While there are a few residues in the Switch II region of Cdc42Hs−PBD46 that have lower-than-average order parameters, the majority of the Switch II residues in the PBD46 construct also have high order parameters. Furthermore, at least one of the residues with a low S^2 has a value for τ_e that reaches the upper bound of τ_m, suggesting an inability to model the motion at this site accurately.

As was the case with Switch I, a number of the residues in Switch II do not appear in the NMR spectrum (Figure 5, white). However, the combination of high order parameters and chemical exchange components (Figure 5, orange and red) observed for Switch II suggests that the mechanism of motional broadening in this region is different from that in Switch I. The chemical exchange relaxation mechanism primarily affects the T_2 relaxation time (eq 4), and does so in a field-dependent manner. However, because the R_{ex} term appears alone in only one of the three relaxation equations, the appearance of chemical exchange components should be treated with caution. In this case, the observed chemical exchange components were produced using several field-dependent values of T_2 and T_1 (Table 1). These exchange components persisted even when an anisotropic motional model was used. Therefore, Switch II does appear to experience chemical exchange, which serves as a different source of motional NMR line broadening than that observed in Switch I. Although there appear to be a greater number of residues experiencing chemical exchange at Switch II for the PBD46 construct (implying increased motion), the fact that more resonances are observable suggests instead that motion in Switch II is more constricted in the PBD46 construct, and that the newly observable residues experience greater chemical exchange broadening in the GDP and GMPPCP constructs. Overall, Switch II appears to be highly ordered on a nanosecond to picosecond time scale, but

experiences dynamic motions on a millisecond to second time scale.

One other aspect of the dynamics at Switch II is particularly interesting. Residues on the inner face and C-terminal end of the α3 helix also experience chemical exchange in the GDP and GMPPCP forms (Figure 5, orange and red residues). However, binding of PBD46 virtually eliminates the exchange in helix α3. The restriction of the chemical exchange in α3 to the inner face of the helix suggests that the unusual dynamics of α3 are a direct result of its proximity to Switch II, rather than a functional involvement of helix α3 in regulator binding. This in turn supports the indication that the PBD46 construct experiences a constriction in motion relative to the GDP and GMPPCP constructs, despite the apparently similar order parameters in all three forms.

Insert. As with Switch II, no noticeable deviation from the mean values of S^2 in the Insert region is observed for any construct. The relatively high order parameters indicate that much like those in Switch II, the residues in the Insert are highly ordered on the nanosecond to picosecond time scale. However, chemical exchange is observed at regions on the body of the protein that are near the Insert in space (residues 86 and 117−119 for GDP and residues 86, 117, and 120 for GMPPCP; orange in Figure 5), suggesting that the entire Insert helix may experience a wagging motion with hinges at these sites. In fact, previous studies have shown that the Insert region does not have strong interactions with the remainder of the protein (as judged by the weak NOE contacts) (*17*). A slow (millisecond) wagging motion such as this may explain the minimal number of NOE contacts between helix αI and the remainder of the protein.

The dynamics of the Insert region change significantly as the protein moves from the inactive (GDP) state through the active (GMPPCP) state into the PBD46-bound state. In particular, the increased flexibility of the Insert in the GDP form is most noticeable, as indicated by the increased complexity of the models required to fit the data in this form (τ_e panel of Figure 4 and Figure 5), and by the relatively long correlation times (∼8−14 ns) observed as compared with other local correlation times in the protein. Motion on such a slow time scale may explain the relatively fast hydrogen−deuterium exchange rates within the insert helix observed in the GDP form of the protein (*17*), and may have important implications for the role of the Insert in interactions with GDI (see the Discussion).

DISCUSSION

We have shown that there are three regions of Cdc42Hs that have dynamics characteristics that are different from those of the bulk of the protein: (1) Switch I, (2) Switch II, and (3) the Insert region. Not only do the characteristics of the dynamic processes differ between regions, but the overall dynamics of the protein also become less complex as it moves from the inactive, GDP-bound form through to the activated, GMPPCP-bound form to the effector (PBD46)-bound form.

Switch I. As we have shown previously (*18*), the effector binding region is comprised primarily of residues in Switch I as well as selected residues in β2. This seems to be a consistent feature of GTP-binding proteins as a similar, but less extensive, binding interface was defined for Ras-RBP (*52*). We show here that residues in Switch I have higher-than-average T_2 times, and lower-than-average NOE values. Deviations from the average values are more pronounced for the GDP and GMPPCP forms than for the PBD46 form. These observations suggest that the residues in Switch I are quite flexible and disordered, but that the flexibility decreases upon binding of PBD46. The dynamics results are consistent with this suggestion. Switch I residues in Cdc42Hs−GDP and Cdc42Hs−GMPPCP are characterized by low order parameters (indicative of high-amplitude motions), and local correlation times on the ∼1 ns time scale. Some residues are flexible enough that they were well fit only by models that included motion on two time scales (<10 ps and 1 ns). However, fewer dynamics parameters (often only S^2) were required to describe the dynamics of the residues in Switch I for Cdc42Hs−PBD46, indicating more constrained motion. Nevertheless, the low order parameters of Switch I residues persist in the PBD46 form, suggesting that the region continues to be flexible although the time scale of motion may be too fast (or too slow) to measure.

Several previous studies have also suggested that the Switch I regions of proteins in the Ras superfamily are disordered. Many resonances in Switch I were unobservable in the NMR spectrum of Cdc42Hs−GDP and Cdc42Hs−GMPPCP forms, presumably due to motional line broadening (*17*, *18*). This was also the case for Switch I residues in Cdc42Hs−PBD46, although to a much lesser extent (*18*). The X-ray crystal structure of Cdc42Hs−GDP (N. Nassar, personal communication) also suggests disorder in Switch I, as evidenced by an increased *B* factor and a less pronounced electron density for this region. Similarly, X-ray crystal structures of RhoA−GDP (*53*) and Rac1−GMPPNP (*54*) indicate reduced order at the effector-binding region. For Ras p21−GDP, Switch I is well ordered, but found at the crystal packing interface, and is therefore likely to be stabilized by intermolecular interactions (*55*). This interpretation is supported by a study of the NMR solution structure and dynamics of Ras p21−GDP, which reveals reduced order and dynamic mobility on the nanosecond time scale at Switch I (*56*). Therefore, we conclude that Switch I is a disordered region that experiences high-amplitude motions on the nanosecond time scale, and that binding of an effector stabilizes these motions to some extent.

Switch II. Switch II also exhibits increased dynamics relative to the remainder of the protein. However, the dynamics characteristics of residues in Switch II are distinct from those of residues in Switch I. Switch II residues in the Cdc42Hs−GDP and Cdc42Hs−GMPPCP constructs are characterized by lower-than-average T_2 values, yet average NOE values. In contrast, these same residues in Cdc42Hs−PBD46 have T_2 (and NOE) values that do not deviate from the average. Nevertheless, the majority of the residues in Switch II in all three constructs have average order parameters and very few, if any, measurable local correlation time components. While high order parameter values are an indication of low-amplitude motion (high degree of local order on the nanosecond to picosecond time scale), they do not necessarily indicate the lack of motion on a different time scale. Negative deviations from average T_2 values are suggestive of additional relaxation mechanisms, such as chemical exchange. Since chemical exchange rates are

strongly field-dependent, measurement of T_2 at several magnetic field strengths should clearly identify or eliminate chemical exchange as a relaxation mechanism. Indeed, the observed chemical exchange components were obtained from T_2 values that were obtained at three fields for the GMPPCP and PBD46 constructs, and at two fields for the GDP construct. To further ensure that the observed chemical exchange components were not an artifact created by the isotropic modeling of protein motion, the GDP construct was also analyzed using an axially symmetric anisotropic model. The results obtained were essentially identical to those obtained using the isotropic model. Furthermore, the axial diffusion ratio was found to be 1.137 (as compared with 1 for a perfect sphere), which suggests that the isotropic model is a good approximation for this protein. Apparently, the residues in Switch II experience significant motion on a much longer time scale (milliseconds) than that characterized by S^2.

Previous studies have painted a contradictory picture of the order in Switch II. In the X-ray crystal structure of RhoA−GDP, Switch II was reported to be primarily helical, although the positions of a few residues in this region were not well-defined (*53*). The crystal structure of Rac1−GMPPNP also revealed well-resolved electron densities for residues in this region. However, Switch II is found at the crystal packing interface in this structure, and may be ordered primarily by intermolecular interactions within the crystal (*54*). In the crystal structure of Cdc42Hs−GDP (N. Nassar, personal communication), two copies of the protein are found in the unit cell. In one copy, Switch II is at the crystal interface and folds into two relatively well-ordered short helices. In the other copy, Switch II is disordered and not stabilized by intermolecular interactions. The fact that short helices are found in crystal structures of Cdc42Hs and other Rho proteins suggests that Switch II exhibits at least partial order when stabilized by intermolecular interactions. There is, however, appreciable evidence for reduced order at Switch II. Milburn et al. (*55*) have suggested that the Switch II region is flexible and sensitive to crystal packing forces in both GDP and GTP analogue forms of H-Ras. Switch II has also been found to be flexible and/or disordered in several Ras crystal structures (*57*), the NMR solution structure of Ras−GDP (*56*), and the NMR solution structure of Cdc42Hs−GDP (*17*). In light of the evidence for chemical exchange presented here, the apparently contradictory observations of order and disorder at Switch II may be explained in terms of conformational exchange between ordered structures. Thus, the crystal structures of these proteins may divulge only one of several ordered conformations of Switch II. In fact, it has been suggested that conformational changes in Switch II are necessary for GDP−GTP exchange, and that a freezing of Switch II into one conformation would prevent the release of bound GDP (*55*). Interestingly, RhoGDI also interacts with Switch II on Cdc42Hs and prevents GDP dissociation (G. R. Hoffman, N. Nassar, and R. A. Cerione, unpublished results; W. Guo, R. E. Oswald, and L. Y. Lian, unpublished results).

In short, this combination of NMR and X-ray data provides a view of Switch II as a well-ordered region of the protein that undergoes conformational exchange on the millisecond time scale between two or more conformations. Like those in Switch I, the motions of residues in Switch II are constricted in part by the binding of PBD46. This is part of a general decrease in the overall flexibility of Cdc42Hs in the effector-bound state. An interesting observation is that the face of the α3 helix that borders Switch II also exhibits chemical exchange dynamics that are similar to those observed for Switch II, suggesting a mode of motion for Switch II that involves movement toward and away from the inner face of helix α3. This is particularly interesting because this region of helix α3 is also involved in GDI binding (G. R. Hoffman, N. Nassar, and R. A. Cerione, unpublished results).

Insert Region. The Insert region is defined relative to other members of the Ras family (*58*). Only the Rho subfamily has this 13-residue insert, and the function of the Insert is not clear. The Insert region contains an α-helix, but the amide protons in the helix are not protected from deuterium exchange on the same time scale as in other helices in the protein (tens of minutes to hours) (*17*). We find here that the Insert experiences increased dynamics in the GDP construct versus the GMPPCP and PBD46 constructs, although the dynamics characteristics are not as pronounced as for Switch I and Switch II.

Three aspects of the increased dynamics of the Insert are most noteworthy. First, the order parameters in the Insert region do not deviate from the protein average, indicating that these residues experience low-amplitude motions on a nanosecond to picosecond time scale in an ordered environment, much the same as for Switch II. Second, residues at the C- and N-terminal portions of the Insert region, as well as residues at the C-terminal end of helix α3 (near the Insert in distance), experience chemical exchange in the GDP and GMPPCP forms, but not in the PBD46 form. This chemical exchange component is strongly suggestive of a hinge motion that allows the helix to move as a block. This is supported by data from crystal structures of Rho family proteins, which show the Insert to be ordered and mobile in Rac1−GTP (*54*), yet ordered and immobile in RhoA−GDP (*53*). As for Switch II, the immobility of the Insert in RhoA was attributed to intermolecular stabilization forces within the crystal. Such concerted motion on the millisecond time scale is consistent with the observed high order parameters on the nanosecond to picosecond time scale for the Insert region. Third, Insert residues in the GDP construct experience different motion within the Insert region than do those in the GMPPCP and PBD46 constructs, as suggested by the increased complexity of the models required to fit the relaxation data of the GDP form and the fairly long time scale motions (∼8−14 ns) of these residues relative to other local motions within the protein. The combination of the hinge motion (millisecond time scale) of the Insert and the slow (nanosecond time scale) motion within the Insert for the GDP form may explain the relatively fast hydrogen−deuterium exchange rates observed for Cdc42Hs−GDP (*17*). In contrast, the Insert residues in the GMPPCP and PBD46 forms experience very fast time scale motions [<10 ps (unobservable) to ∼2 ns]. Although the hinge motion persists in the GMPPCP form, there is a clear decrease in the complexity in the dynamics of this region in this form and in the PBD46 form versus that in the GDP form.

Recent studies have shown that the Insert region mediates the interaction of Rac (another member of the Rho subfamily) with NADPH oxidase (*14*, *59*). Several lines of evidence

suggest that the Insert region is also important in various physiological functions of Cdc42Hs. For example, removal of the Insert region does not affect the binding of RhoGDI (binding is likely to be mediated by the prenylated C-terminus of Cdc42Hs and interactions with Switch II) but does eliminate the ability of RhoGDI to affect the dissociation of GDP. While this may be due to other changes in the structure of the protein produced by the removal of the Insert (W. Guo and R. E. Oswald, unpublished results), the potential role of the Insert cell signaling and oncogenesis is highlighted by the observation that the F28L fast cycling mutant of Cdc42Hs is capable of transforming cells, but that the F28L mutant of the Cdc42Hs with the Insert removed is no longer capable of cell transformation (*16*). One possible interpretation of these results is that an as yet to be discovered effector on the pathway for cell transformation binds to the Insert region (*16*). However, no chemical shift changes are seen in the Insert region upon exchange of GDP for GMPPCP (*17*). Rather, the observed changes in the dynamics of the Insert region in different forms of the protein suggest that it is the dynamics and not the structure that is important for the functional contribution of this region of the protein in different signaling states.

The recurring theme of this study is that dynamic motion is correlated with the function of Cdc42Hs. Different types of segmental flexibility are observed in all three regions of the protein that are important for function. Furthermore, this flexibility is decreased upon binding of effector. Interestingly, the PBD46 peptide is not well-structured in the absence of Cdc42Hs (W. Guo and R. E. Oswald, unpublished results), suggesting that the binding of PBD46 results in a decrease in entropy for both the peptide and Cdc42Hs. Although this in itself would be energetically unfavorable, presumably the flexibility in the unbound form allows the protein to maximize the binding enthalpy at the interface, overcoming the unfavorable entropic contribution.

Dynamics have been shown to be important components of binding energy in a variety of other systems. Side chain dynamics in the phosphopeptide binding site of the phospholipase $C_{\gamma 1}$ SH_2 domain is an important determinant of binding energy (*60*). Likewise, the dynamic character of the "flaps" in the HIV protease as well as the flexible loop in the active site (*22*) plays an important role in binding substrate, catalysis, and the release of product. Protein dynamics seems also to be important in the binding of the drug Taxol to the antiapoptotic protein Bcl-2 in that the binding domain is a disordered, regulatory loop (*61*). In the case of bacterial amino acid binding proteins (*62*) and, most likely, glutamate receptors (*63*, *64*), the unbound state consists of two rather flexible lobes that close to surround the bound amino acid. Conformational flexibility is also an important characteristic of the function of many DNA binding proteins, such as the trp repressor (*65*) and the cMyb DNA binding domain (*66*). The widespread observation that regions of proteins that are involved in important functional interactions are flexible suggests that this may be a general mechanism by which proteins maximize the enthalpy of binding.

ACKNOWLEDGMENT

We thank the Laboratory of Chemical Physics at the National Institutes of Health and Drs. Dan Garrett and Frank Delaglio for making available the programs PIPP and NMRPipe which were useful in analyzing our NMR data. We are also grateful to Prof. Gerhard Wagner and Greg Heffron (Harvard Medical School) for the use of their Varian Unity Plus 400 spectrometer. We thank Norma Pawley, Jeffrey Reinking, Michael Sutcliffe, Richard Cerione, Greg Weiland, Nicolas Nassar, and Dawit Gizachew for helpful discussions.

SUPPORTING INFORMATION AVAILABLE

Three tables of relaxation data at all fields for Cdc42Hs−GDP, −GMPPCP, and −PBD46 and three tables of dynamics results from isotropic Modelfree, version 4.0, analyses for Cdc42Hs−GDP, −GMPPCP, and −PBD46. This material is available free of charge via the Internet at http://pubs.acs.org.

REFERENCES

1. Bourne, H. R., Sanders, D. A., and McCormick, F. (1991) *Nature 349*, 117−127.
2. Bos, J. L. (1989) *Cancer Res. 49*, 4682−4689.
3. Wittinghofer, A. (1998) *Biol. Chem. Hoppe-Seyler 379*, 933−937.
4. Cerione, R. A., and Zheng, Y. (1996) *Curr. Opin. Cell Biol. 8*, 216−222.
5. Lin, R., Bagrodia, S., Cerione, R., and Manor, D. (1997) *Curr. Biol. 7*, 794−797.
6. Hart, M. J., Eva, A., Evans, T., Aaronson, S. A., and Cerione, R. A. (1991) *Nature 354*, 311−314.
7. Horii, Y., Beeler, J. F., Sakaguchi, K., Tachibana, M., and Miki, T. (1994) *EMBO J. 13*, 4776−4786.
8. Hart, M. J., Shinjo, K., Hall, A., Evans, T., and Cerione, R. A. (1991) *J. Biol. Chem. 266*, 20840−20848.
9. Barfod, E. T., Zheng, Y., Kuang, W. J., Hart, M. J., Evans, T., Cerione, R. A., and Ashkenazi, A. (1993) *J. Biol. Chem. 268*, 26059−26062.
10. Leonard, D., Hart, M. J., Platko, J. V., Eva, A., Henzel, W., Evans, T., and Cerione, R. A. (1992) *J. Biol. Chem. 267*, 22860−22868.
11. Rittinger, K., Walker, P. A., Eccleston, J. F., Nurmahomed, K., Owen, D., Laue, E., Gamblin, S. J., and Smerdon, S. J. (1997) *Nature 388*, 693−707.
12. Nassar, N., Hoffman, G. R., Manor, D., Clardy, J. C., and Cerione, R. A. (1998) *Nat. Struct. Biol. 5*, 1047−1052.
13. Nomanbhoy, T. K., Leonard, D. A., Manor, D., and Cerione, R. A. (1996) *Biochemistry 35*, 4602−4608.
14. Freeman, J. L., Abo, A., and Lambeth, J. D. (1996) *J. Biol. Chem. 271*, 19794−19801.
15. McCallum, S. J., Wu, W. J., and Cerione, R. A. (1996) *J. Biol. Chem. 271*, 21732−21737.
16. Wu, W. J., Lin, R., Cerione, R. A., and Manor, D. (1998) *J. Biol. Chem. 273*, 16655−16658.
17. Feltham, J. L., Dötsch, V., Raza, S., Manor, D., Cerione, R. A., Sutcliffe, M. J., Wagner, G., and Oswald, R. E. (1997) *Biochemistry 36*, 8755−8766.
18. Guo, W., Sutcliffe, M. J., Cerione, R. A., and Oswald, R. E. (1998) *Biochemistry 37*, 14030−14037.
19. Abdul-Manan, N., Aghazadeh, B., Liu, G. A., Majumdar, A., Ouerfelli, O., Siminovitch, K. A., and Rosen, M. K. (1999) *Nature 399*, 379−383.
20. Mott, H. R., Owen, D., Nietlispach, D., Lowe, P. N., Manser, E., Lim, L., and Laue, E. D. (1999) *Nature 399*, 384−388.
21. Kay, L. E., Torchia, D. A., and Bax, A. (1989) *Biochemistry 28*, 8972−8979.
22. Nicholson, L. K., Grzesiek, S., Yamazaki, T., Stahl, S. J., Kaufman, P. T., Wingfield, P. T., Domaille, P. J., Bax, A., and Torchia, D. A. (1995) *Nat. Struct. Biol. 2*, 274−280.
23. Clore, G. M., Driscoll, P. C., Wingfield, P. T., and Gronenborn, A. M. (1990) *Biochemistry 29*, 7387−7401.

24. Stone, M. J., Fairbrother, W. J., Palmer, A. G., III, Reizer, J., Saier, M. H., Jr., and Wright, P. E. (1992) *Biochemistry 31*, 4394−4406.
25. Schneider, D. M., Dellwo, M. J., and Wand, J. A. (1992) *Biochemistry 31*, 3645−3652.
26. Barbato, G., Ikura, M., Kay, L. E., Pastor, R. W., and Bax, A. (1992) *Biochemistry 31*, 5269−5278.
27. Marion, D., Driscoll, P. C., Kay, L. E., Wingfield, P. T., Bax, A., Gronenborn, A., and Clore, G. M. (1989) *Biochemistry 28*, 6150−6156.
28. States, D. J., Haberkorn, R. A., and Ruben, D. J. (1982) *J. Magn. Reson. 48*, 286−292.
29. Delaglio, F., Grzeseik, S., Vuister, G., Zhu, G., Pfeifer, J., and Bax, A. (1995) *J. Biomol. NMR 6*, 277−293.
30. Kay, L. E., Keifer, P., and Saarinen, T. (1992) *J. Am. Chem. Soc. 114*, 10663−10665.
31. Garrett, D. S., Powers, R., Gronenborn, A. M., and Clore, G. M. (1991) *J. Magn. Reson. 95*, 214−220.
32. Kay, L. E., Nicholson, L. K., Delaglio, F., Bax, A., and Torchia, D. A. (1992) *J. Magn. Reson. 97*, 359−375.
33. Farrow, N. A., et al. (1994) *Biochemistry 33*, 5984−6003.
34. Peng, J. W., Thanabal, V., and Wagner, G. (1991) *J. Magn. Reson. 95*, 421−427.
35. Grzesiek, S., and Bax, A. (1993) *J. Am. Chem. Soc. 115*, 10663−10665.
36. Nicholson, L. K., Kay, L. E., Baldisseri, D. M., Arango, J., Young, P. E., Bax, A., and Torchia, D. A. (1992) *Biochemistry 31*, 5253−5263.
37. Davis, D. G., Perlman, M. E., and London, R. E. (1994) *J. Magn. Reson. B104*, 266−275.
38. Tjandra, N., Wingfield, P., Stahl, S., and Bax, A. (1996) *J. Biomol. NMR 8*, 273−284.
39. Abragam, A. (1961) *Principles of Nuclear Magnetism*, pp 264−353, Clarendon Press, Oxford, U.K.
40. Lipari, G., and Szabo, A. (1982) *J. Am. Chem. Soc. 104*, 4546−4559.
41. Keiter, E. A. (1986) Ph.D. Thesis, University of Illinois, Urbana, IL.
42. Hiyama, Y., Niu, C.-H., Silverton, J. V., Bavoso, A., and Torchia, D. A. (1988) *J. Am. Chem. Soc. 110*, 2378−2383.
43. Szyperski, T., Neri, D., Leiting, B., Otting, G., and Wüthrich, K. (1992) *J. Biomol. NMR 2*, 323−334.
44. Farrar, T. C., and Becker, E. D. (1971) in *Fourier Transform NMR Spectroscopy*, pp 1−115, Academic Press, New York.
45. Lipari, G., and Szabo, A. (1982) *J. Am. Chem. Soc. 104*, 4559−4570.
46. Clore, G. M., Bax, A., Driscoll, P. C., Wingfield, P. T., and Gronenborn, A. M. (1990) *Biochemistry 29*, 8172−8184.
47. Mandel, A. M., Akke, M., and Palmer, A. G., III (1995) *J. Mol. Biol. 246*, 144−163.
48. Palmer, A. (1998) *ModelFree*, version 4.0, http://cpmcnet.columbia.edu/dept/gsas/biochem/labs/palmer.
49. Shoemaker, D. P., Garland, C. W., and Nibler, J. W. (1996) *Experiments in Physical Chemistry*, 6th ed., pp 722−724, McGraw-Hill, New York.
50. Jin, D., Andrec, M., Montelione, G. T., and Levy, R. M. (1998) *J. Biomol. NMR 12*, 471−492.
51. Fushman, D., Cahill, S., and Cowburn, D. (1997) *J. Mol. Biol. 266*, 173−194.
52. Nassar, N., Horn, G., Herrmann, C., Scherer, A., McCormick, F., and Wittinghofer, A. (1995) *Nature 375*, 554−560.
53. Wei, Y., Zhang, Y., Derewenda, U., Liu, X., Minor, W., Nakamoto, R. K., Somlyo, A. V., Somlyo, A. P., and Derewenda, Z. S. (1997) *Nat. Struct. Biol. 4*, 699−703.
54. Hirshberg, M., Stockley, R. W., Dodson, G., and Webb, M. R. (1997) *Nat. Struct. Biol. 4*, 147−152.
55. Milburn, M. V., Tong, L., DeVos, A. M., Brunger, A., Yamaizumi, Z., Nishimura, S., and Kim, S. (1990) *Science 247*, 939−945.
56. Kraulis, P. J., Domaille, P. J., Campbell-Burk, S. L., VanAken, T., and Laue, E. D. (1994) *Biochemistry 33*, 3515−3531.
57. Wittinghofer, A., and Pai, E. (1991) *Trends Biochem. Sci. 16*, 382−387.
58. Sutcliffe, M. J., Feltham, J., Cerione, R. A., and Oswald, R. E. (1994) *Protein Pept. Lett. 1*, 84−91.
59. Joneson, T., and Bar-Sagi, D. (1998) *J. Biol. Chem. 273*, 17991−17994.
60. Pascal, S. M., Singer, A. U., Gish, G., Yamazaki, T., Shoelson, S. E., Pawson, T., Kay, L. E., and Forman-Kay, J. D. (1994) *Cell 77*, 461−472.
61. Rodi, D. J., Janes, R. W., Sanganee, H. J., Holton, R. A., Wallace, B. A., and Makowski, L. (1999) *J. Mol. Biol. 285*, 197−203.
62. Oh, B. H., Pandit, J., Kang, C. H., Nikaido, K., Gokcen, S., Ames, G. F. L., and Kim, S. H. (1993) *J. Biol. Chem. 268*, 11348−11355.
63. Armstrong, N., Sun, Y., Chen, G. Q., and Gouaux, E. (1998) *Nature 395*, 913−917.
64. Sutcliffe, M. J., Wo, Z. G., and Oswald, R. E. (1996) *Biophys. J. 70*, 1575−1589.
65. Gryk, M. R., Jardetzky, O., Klig, L. S., and Yanofsky, C. (1996) *Protein Sci. 5*, 1195−1197.
66. Ogata, K., et al. (1996) *Nat. Struct. Biol. 3*, 178−187.
67. Bodenhausen, G., and Ruben, D. J. (1980) *Chem. Phys. Lett. 69*, 185−189.
68. Barton, G. J. (1993) *Protein Eng. 6*, 37−40.

BI9913707